Novel Pattern Formation in Granular Matter*

Hernán A. Makse[1], Shlomo Havlin[1,2], Peter R. King[3], and H. Eugene Stanley[1]

[1] Center for Polymer Studies and Dept. of Physics, Boston University, Boston, MA 02215 USA
[2] Department of Physics, Bar-Ilan University, Ramat Gan, ISRAEL
[3] BP Exploration Operating Company Ltd., Sunbury-on-Thames, Middx., TW16 7LN, UK

Abstract. Sedimentary rocks have complicated permeability patterns arising from the geological processes that formed them. We concentrate on pattern formation in one particular geological process, avalanches (grainflow) in windblown or fluvial sands. We present a simple experiment and numerical model of how these avalanches cause segregation in particle size that lead to characteristic laminated patterns. We also address the longstanding question of how such patterns are generated. We analyze data on two sandstone samples from different, but similar, geological environments, and find that the permeability fluctuations display long-range power-law correlations characterized by an exponent H. For both samples, we find $H \approx 0.82 - 0.90$. These permeability fluctuations significantly affect the flow of fluids through the rocks. We demonstrate this by investigating the influence of long-range correlation on percolation properties, like cluster morphology, and relate these properties to characteristics important for hydrocarbon recovery such as breakthrough time for injected fluids and recovery efficiency.

1 Introduction

Sedimentary rocks have complex correlated patterns that influence the flow and recovery of hydrocarbons. These patterns arise from the complicated geological processes that formed the rocks. It is a major experimental and theoretical challenge to understand how the process forms the patterns. For oil companies it is also extremely important to understand how the patterns influence recovery and to make quantitative predictions of the influence.

In this paper we address the following points:

(i) The formation of periodic laminae of fine and coarse grains in sedimentary structures is a widespread phenomenon (Bagnold 1941, McKee et al. 1967, Jopling and Walker 1968, Borges 1975, Fryberger and Schenk 1981, Cheel and Middleton 1986, Hunter 1985, Buck 1985), its origin remains an open question. Figure 1a shows a section of a Triassic, planar cross bedded Aeolian sandstone from Lochabriggs near Dumfries, Scotland where a typical example of stratification pattern is observed. We

* Dedicated to Professor W. Ebeling on the Occasion of his 60th Birthday.

address the longstanding question of how such periodic patterns are generated by proposing a "table top" experiment Makse et al. 1995b. The experiment reproduces the successive layers of fine and coarse particles observed in sedimentary structures.

(ii) We confirm the spatial patterns predicted with the experiment by comparing with real rock samples. Figure 2 shows the result of the experiment Makse et al. 1995b. The size segregation into alternating layers is quite similar to that found in the geological sample and in stratigraphic records. We note two features:
   (a) **Alternation.** We clearly see the formation of alternating layers consisting of small and large particles.
   (b) **Segregation.** We observe that the layers are built up in such a way that small particles are segregated in layers near the top of the slip-face, while larger particles form layers near the substrate at the bottom.

(iii) We quantify the spatial correlations in rocks. Permeability in sandstone can change by many orders of magnitude over very short distances. Not only are there large fluctuations in permeability but the permeability can exhibit strong anisotropy. Deriving methods to describe these spatial patterns is a major challenge. Both the efficient recovery of hydrocarbon and contaminant dispersal and control in ground water is affected by the understanding of such spatial patterns. Traditionally these patterns have been modeled with a finite range correlation scale. We analyze a detailed permeability map and show that the data are consistent with a long-range correlation model.

2 Rock Slab Data

The Aeolian sandstone shown in Fig. 1a was formed by windblown sand (Bagnold 1941). A small sand accumulation (sand bar or dune) is formed as the unidirectional wind moves material along the bed. As the wind continues, sand is moved from the upstream side of the dune to the crest of the dune, and the slope of the sand bar become steeper. When the initial dune reaches a critical angle or slope, a downstream slip-face is developed where avalanches of sand begins. After this, new material is brought to the top of the dune until another avalanche occurs. The evidence of such sedimentary process can be traced in the layered structure of the Lochabriggs sample of Fig. 1a.

3 Experiment

To understand the origin of the layering segregation we begin by developing the following "table-top" experiment (Makse et al. 1995b). The experimental

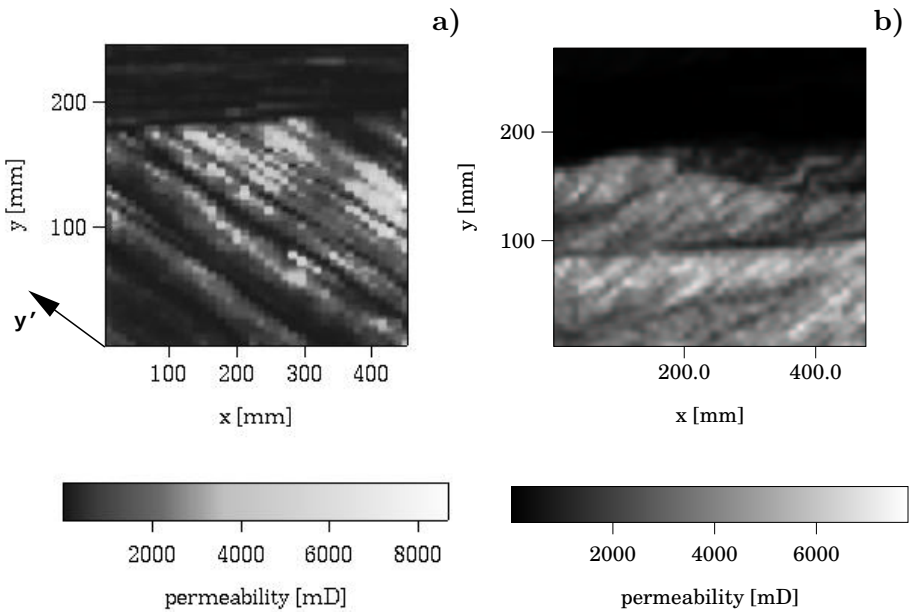

Fig. 1. (a) Permeability map of the Lochabriggs sample. The complete sample consists of two slabs of 448 mm by 246 mm and 10 mm thick, and again only three faces were used in this study. The permeability was measured every 12 mm and 4 mm in the x and y directions, respectively, so that a grid of $n_x = 38$ by $n_y = 61$ was obtained. Notice the strong anisotropy of this sample manifested by the crests elongated along the y' direction. (b) Permeability map of the Hollington sample. The complete sample consist of two slabs, measuring 474 mm by 276 mm and 10 mm thick. Three faces at heights $z = 0$, $z = 10$, and $z = 20$ mm were used to study the permeability pattern (the $z = 0$ face is shown in this figure). Unfortunately the measurements of one face were corrupted by instrumentation error and so only three faces could be used. The permeability was measured every 10 mm in the x direction and every 4 mm in the y direction, so a grid of $n_x = 48$ by $n_y = 69$ permeability values was obtained.

setup consists of a vertical Hele-Shaw (Hele-Shaw 1898) cell with a gap of 5mm separating two transparent plates of 300mm by 200mm (see Fig. 2). We close the left edge of the cell leaving the right edge free, and we pour, next to the left edge, an equal-volume mixture of white fine silica sand (typical size 0.4mm) and dark coarse sugar crystals (typical size 0.9mm). We choose this quasi-two-dimensional geometry since the actual geological system is translationally invariant along the transverse direction (due to the unidirectional flow of sand).

Figure 2 shows the result of the experiment. We note the two main features Makse et al. 1995b: (a) alternation, and (b) segregation.

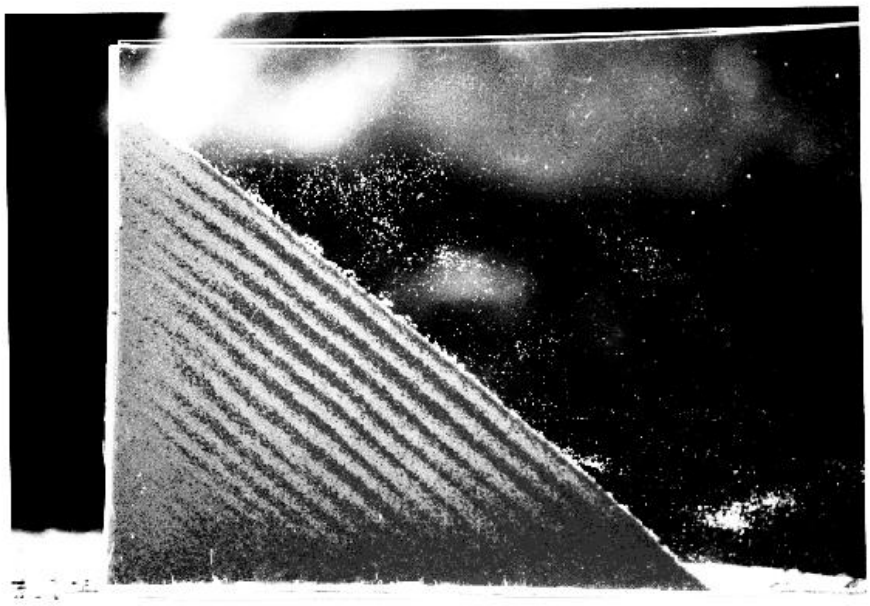

Fig. 2. Photograph of the experimental sandpile showing the periodic layers.

We developed a model that displays stratification of the large and small grains in alternating layers Makse et al. 1996b. We found that the key requirement for self-stratification is a difference in the repose angles of the two pure species, a prediction confirmed by experimental findings of Makse et al. 1995b. We also identified a kink mechanism to describe the dynamics of self-stratification.

4 Spatial Correlations and Connectivity

Next we discuss spatial patterns in permeable rocks. We analyzed two samples: one the *aeolian* Lochabriggs (Lo) sample shown in Fig. 1a, and the second sample a Triassic, *fluvial* trough cross bedded sandstone from Hollington (Ho) near Stafford in the East Midlands of England (Fig. 1b) (Makse et al. 1996a). The deposition process is similar. Now the grains are deposited under

water. Eddying on the slip face of the sand bar influences the avalanching slightly.

Permeability on the small scale of both rock samples was measured by standard mini-permeametry (Makse et al. 1996a, Halvorsen and Hurst 1990). The mini-permeameter is a tube through which a gas (air in laboratory measurements) is blown into the rock sample at a fixed pressure. The flow rate of the gas into the rock sample is measured. The permeability k is then the ratio of the flow rate Q to the pressure drop ΔP (which is applied pressure minus atmospheric pressure) multiplied by the viscosity of the gas μ.

$$k \equiv -\frac{\mu Q}{\Delta P}. \tag{1}$$

Corrections must be made for the compressibility of the gas and the flow geometry, which is hemispherical from the injection point. The end of the permeameter in contact with the rock is made of a flexible plastic ring to ensure a good seal. The probe comes in a variety of sizes to measure permeability fluctuations on different length scales; for our measurements the probe had a 1 cm diameter.

The permeability maps so obtained are shown in Figs. 1a and 1b. By inspection, we see that local permeability varies significantly within a very short length scale, suggesting that the permeability may not be an independent random process.

We plot the permeability histograms for the Sample Ho in Fig. 3. The high permeability zone has a typical permeability of 3300 mD, the low permeability zone has a typical permeability of 30 mD. Local permeability is proportional to the square of the grain radius for uncompacted, well sorted, clean, quartzite sandstone. The high permeability zone consists of interbedded fine and coarse grain material and hence has a much higher variability. The low permeability zone is more homogeneous, consisting of more exclusively fine grained material.

Next we measure the spatial correlations in permeability. We study the correlations of the permeability field $k(i,j)$ $(i,j = 1,...,n_x,n_y)$ along the x and y directions (see Fig. 1). To this end, we first integrate the permeability variables along both directions separately, by calculating the "net displacements" $x_j(\ell)$ and $y_i(\ell)$

$$x_j(\ell) \equiv \sum_{i=1}^{\ell} (k(i,j) - \overline{k(j)}) \qquad [j = 1,...,n_y], \tag{2}$$

and

$$y_i(\ell) \equiv \sum_{j=1}^{\ell} (k(i,j) - \overline{k(i)}) \qquad [i = 1,...,n_x], \tag{3}$$

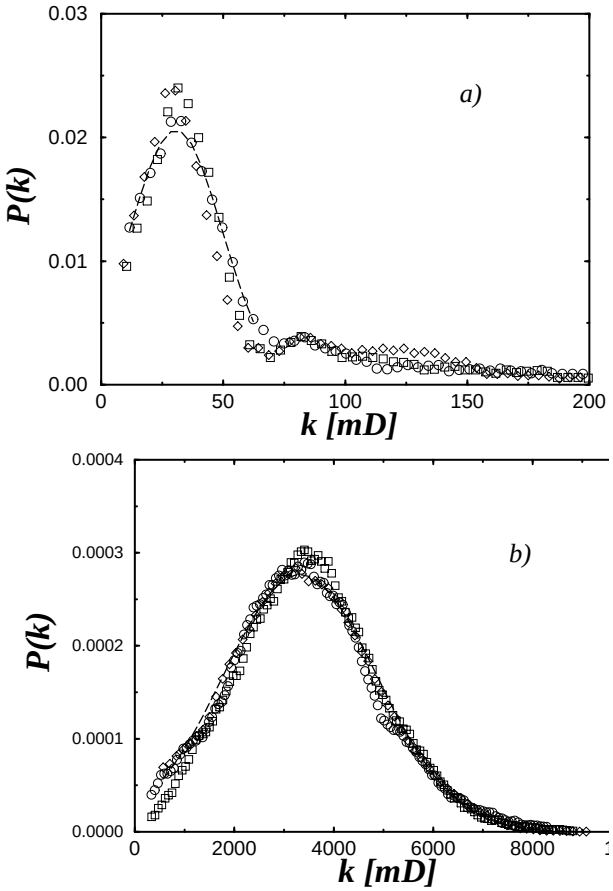

Fig. 3. Normalized permeability distributions for the Sample Ho corresponding to (a) low permeability zone, and (b) high permeability zone. In both figures we plot the distributions corresponding to three different faces of the sample. The distributions are fitted by Gaussian functions. We notice the large difference in the mean value of the permeability between the low and high permeability zones.

where $\overline{k(j)} = (1/n_x)\sum_{i=1}^{n_x} k(i,j)$ and $\overline{k(i)} = (1/n_y)\sum_{j=1}^{n_y} k(i,j)$ [1]. Then we calculate the variance $V_x(\ell) \equiv \langle \overline{x(\ell)^2} - \overline{x(\ell)}^2 \rangle^{1/2}$ and $V_y(\ell) \equiv \langle \overline{y(\ell)^2} - \overline{y(\ell)}^2 \rangle^{1/2}$ as a function of the lag ℓ The scaling behavior of the variance

$$V_x(\ell) \sim \ell^{H_x} \quad , \qquad V_y(\ell) \sim \ell^{H_y} \tag{4}$$

can distinguish between short and long range correlations. For uncorrelated

[1] The spatial average over a window of size ℓ is denoted by the overbar, and the disorder average over different displacements (x_j and y_i) is denoted by the angular brackets.

permeability variables, $H = 1/2$, while $1/2 < H < 1$ implies persistent long-range correlations among the variables. The correlation exponent H describes the "roughness of the permeability landscape" (Vicsek 1992, Barabasi and Stanley 1995, Family and Vicsek 1991)[2]

The method described so far is called rms fluctuation analysis which however, is known to fail if *(i)* the signal is nonstationary (Peng et al. 1994), or *(ii)* the signal is highly correlated $H \simeq 1$ (Leschhorn and Tang 1993, Makse and Amaral 1995). In case *(i)*, the rms method detects spurious correlations due to the patchiness of the signal (Peng et al. 1994), while in case *(ii)* the rms method gives smaller effective exponents (in particular when small samples are used) because the variance has an upper bound $V(\ell) < \ell$ and therefore the method cannot detect fluctuations with exponent $H \geq 1$ (Leschhorn and Tang 1993, Makse and Amaral 1995). In our case we find that, apart from possible nonstationarities, the permeability values are strongly correlated.

To overcome the limitations of the rms method, we will analyze the spatial correlations of the permeability by using detrended fluctuation analysis (DFA) (Peng et al. 1994) and wavelet analysis (Muzy et al. 1991, Arneodo et al. 1995). The DFA method (Peng et al. 1994) consists of subtracting the local trend (defined as the ordinate of a linear least-squares fit to the permeability values) in each window of size ℓ defined in (2,3).

The wavelet transform (WT) of a given function $f(x)$ is defined as

$$T_\Psi(x_0, a) \equiv \frac{1}{a} \int_{-\infty}^{\infty} f(x)\, \Psi\left(\frac{x - x_0}{a}\right)\, dx, \tag{5}$$

where Ψ is the analyzing wavelet, x_0 the translation parameter, and a the scale parameter. After performing the WT with a given wavelet, we can determine the values $x_i(a)$ at which T_Ψ has local extrema. The sum of the absolute values of the local extrema raised to the power q exhibits power law dependence on the scale a,

$$Z(a, q) \equiv \sum_{\{x_i(a)\}} |T_\Psi(x_i(a), a)|^q \;\sim\; a^{\tau(q)}, \tag{6}$$

defining the exponent $\tau(q)$.

The function $Z(a, q)$ is directly related to the scaling properties of the $q-$th moment of the signal $f(x)$. For certain values of q, the exponents $\tau(q)$ have known meaning. In particular $\tau(2)$ is related to the scaling exponent of the Fourier power spectra: $S(f) \sim f^{-\beta}$ with $\beta = 2 + \tau(2)$, and therefore

$$\tau(2) = 2H - 1. \tag{7}$$

[2] The exponent H is called the Hurst exponent for the associated fractional Brownian motions (fBm) $x_j(\ell)$ and $y_i(\ell)$ defined by Eq. (2,3). However, we must note that the original permeability $k(i, j)$ is fractional Gaussian noise (fGn). Therefore, in a numerical study of the effect of long-range correlations in porous media, we must generate the permeability values from a fGn and not from a fBm.

Thus $\tau(2) > 0$ indicates the presence of long-range correlations ($H > 1/2$), and $\tau(2) = 0$ ($H = 1/2$) indicate the absence of correlations. The wavelet method is free from restrictions related to nonstationarities and to the presence of large correlations (Muzy et al. 1991, Arneodo et al. 1995).

The results for the permeability correlations for the Sample Ho are shown in Fig. 4. In Fig. 4a, we show the correlations for both high and low permeability zones, measured in the x and y directions. In this case, before calculating the variance, the permeability is normalized by dividing by the standard deviation calculated independently for each direction. The data are consistent with power-law correlations; using the DFA method, we find

$$H_x = 0.89 \pm 0.06 \qquad H_y = 0.90 \pm 0.06. \qquad \text{[Ho: DFA]} \qquad (8)$$

Results for the correlations along the x direction are shown separately for the high and low permeability zones in Fig. 4b. The correlations are satisfactorily modeled by a power law where $H_x \simeq 0.89$, independent of the magnitude of the overall permeability. These values are confirmed, within the error bars, using the wavelet analysis. We find that

$$H_x = 0.82 \pm 0.06 \qquad H_y = 0.84 \pm 0.06. \qquad \text{[Ho: Wavelet]} \qquad (9)$$

As seen in Fig. 1a, the high permeability zone of sample Lo presents strong anisotropy with anisotropic axes (x', y') not coincident with the coordinate frame (x, y) (see Fig. 1a). We calculate the variance along the y' direction (parallel to the direction of the crests) and find (Fig. 5) using the DFA method

$$H_{y'} = 0.85 \pm 0.06, \qquad \text{[Lo: DFA]} \qquad (10)$$

a value that is consistent with our findings for the Sample Ho. Using wavelet analysis, we find

$$H_{y'} = 0.84 \pm 0.06. \qquad \text{[Lo: Wavelet]} \qquad (11)$$

Along the x' direction a periodic morphology is observed with a wave length of about 60 mm. This introduces a characteristic length scale so that no scale invariance power law correlations are expected along this direction. The existence of this laminar periodic structure is consistent with a depositional model of sand dune dynamics (Makse et al. 1995b).

Thus for both methods we find that $H > 1/2$, thereby demonstrating the presence of long-range correlations in the Ho and Lo samples.

5 Model

We incorporate the spatial correlation properties of real systems into the framework of the percolation problem (Bunde and Havlin, 1994), to investigate the effects that this has on the various quantities of interest, and to consider the consequent implications.

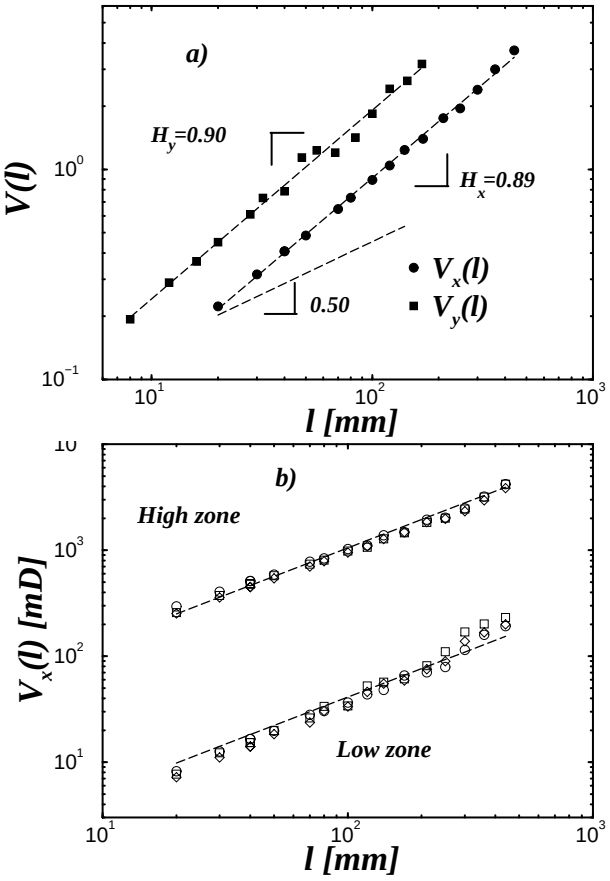

Fig. 4. Log-log plot of the variances of the permeability calculated using the DFA method for the sample Ho. (*a*) Variances $V_x(\ell)$ and $V_y(\ell)$ along the x and y directions respectively, averaged over the three different faces of the sample, and averaged over the high and low permeability zones together for $V_x(\ell)$ and over the high permeability zone for $V_y(\ell)$. The power law relationship between the variance and the separation distance ℓ is characterized by exponents $H_x = 0.89 \pm 0.06$ and $H_y = 0.90 \pm 0.06$. The exponents are the same within error bars indicating the isotropy of the correlations in the xy plane. (*b*) Variance $V_x(\ell)$ calculated along the x direction for the high and low permeability zones, separately. Data are averaged over the three different faces of the sample. Both set of data are consistent with a power law $H_x \simeq 0.89$, showing that the spatial correlations are the same in both zones.

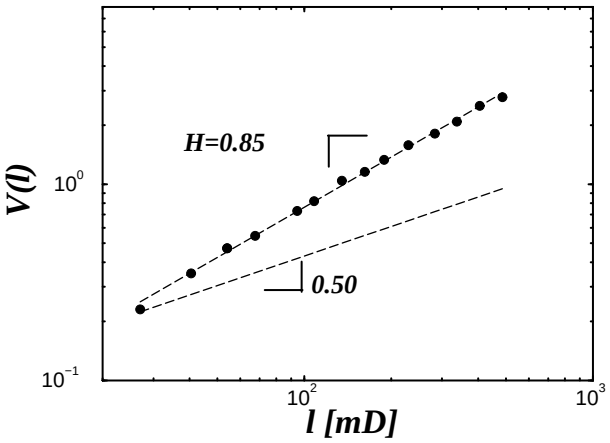

Fig. 5. Log-log plot of the variance calculated along the y' for the high permeability zone of Sample Lo, averaged over the three different faces of the sample. Along the y' direction, a correlation exponent of $H = 0.85 \pm 0.06$ is found. However, along the x' direction, a periodic pattern is observed. Thus the anisotropy in this sample is manifested in a change of behavior from long-range correlation scaling along y' to periodic morphology along x'.

As an example, imagine an oil reservoir made from a river system. The old river channels represent good sand with high permeability. The other rock (shale) has poor permeability. Hence, for many purposes it can be modeled by a conductor/insulator or percolation system. The sand bodies may be thought of as some shapes distributed in space. They may tend to avoid each other or stack next to each other. Fortunately for the petroleum industry, they may also overlap, so it is possible for large "clusters" of sand bodies to exist.

In order to quantify these ideas, we consider the *correlated* percolation model (Coniglio et al. 1977, Weinrib 1984, Prakash et al. 1992, Makse et al. 1995a, Pang et al. 1995). In the limit where correlations are so small as to be negligible a site in the square lattice is occupied *at random* with a probability p (Bunde and Havlin, 1994). However, the fact that we find *spatial correlations* in the rock suggest that the process can be better modeled using the correlated percolation model where each site is not independently occupied, but is occupied with a probability that depends on the occupancy of the neighborhood. For a method of generating long-range correlations, see Makse et al. 1995c. We analyse the structural and dynamic properties of the resulting connected structure. It is worth noting that the percolation model applies not only to the scale of the pore structure but also to larger scales such as the lamination scale. For both the discrete (sand/shale) and continuous systems (permeability), it is important to know how long-range correlations

influence the macroscopic connectivity and flow.

The impact of correlations is apparent from Fig. 6. Figure 6a is for conventional uncorrelated percolation, and Fig. 6b is for percolation with long-range scale-invariant correlations. Both figures are plotted at the critical concentration p_c, above which fluid can flow since there exists an "incipient infinite cluster" that forms just when a connected path breaks through. The occupancy probability p corresponds to the net to gross or volume fraction of good sand in actual sand systems. It is apparent by visual inspection that the clustering properties for the two cases differ dramatically. For example, by comparing Figs. 6a and 6b, we see that the clusters are much larger and more compact in the case of long-range correlations. This implies that there are fewer dead-ends and hence less unswept oil. Therefore, the recovery percentage increases for such strongly correlated systems. Our preliminary results indicate an increase of about 10% in the recovery percentage of correlated systems in comparison with uncorrelated systems.

Figure 7 shows the changes with the correlation exponent γ of the fractal dimension of the minimum path, d_{min} (the shortest path that one can get through the cluster from one to the other). The correlation exponent γ measures the degree of correlation in the system, being uncorrelated for $\gamma = 2$ and strongly correlated for $\gamma = 0$. Again we see a striking dependence of this property upon the degree of correlations. The fractal dimension of the minimum path approaches one (the minimum path becomes equal to the Euclidian distance between the points) as $\gamma \to 0$ (strong correlations), meaning that the cluster becomes more compact in agreement with the above behavior. The fact that the shortest streamlines are "straighter" leads to shorter breakthrough times. As the tortuosity of the streamlines is reduced, we expect dispersion of the front to be reduced and hence better recovery efficiency.

Similar analyses have been performed with other quantities characterizing the connectivity properties of the percolation clusters. For example we find that the critical concentration p_c increases as a function of γ. Therefore one would expect better overall connectivity at lower net to gross in the correlated case than in the uncorrelated case. The quantitative changes with the degree of correlations indicate the errors that are being made with currently-used uncorrelated models.

6 Method of Generating Long-Range Correlations

One of the most used methods to generate a sequence of random numbers with power-law correlations is the Fourier filtering method (Ffm) (Prakash et al. 1992, Saupe 1988, Feder 1988, Peng et al. 1991). It consists of filtering the Fourier components of a uncorrelated sequence of random numbers with a suitable power-law filter in order to introduce correlations among the variables. This method has the disadvantage of presenting a finite cutoff in

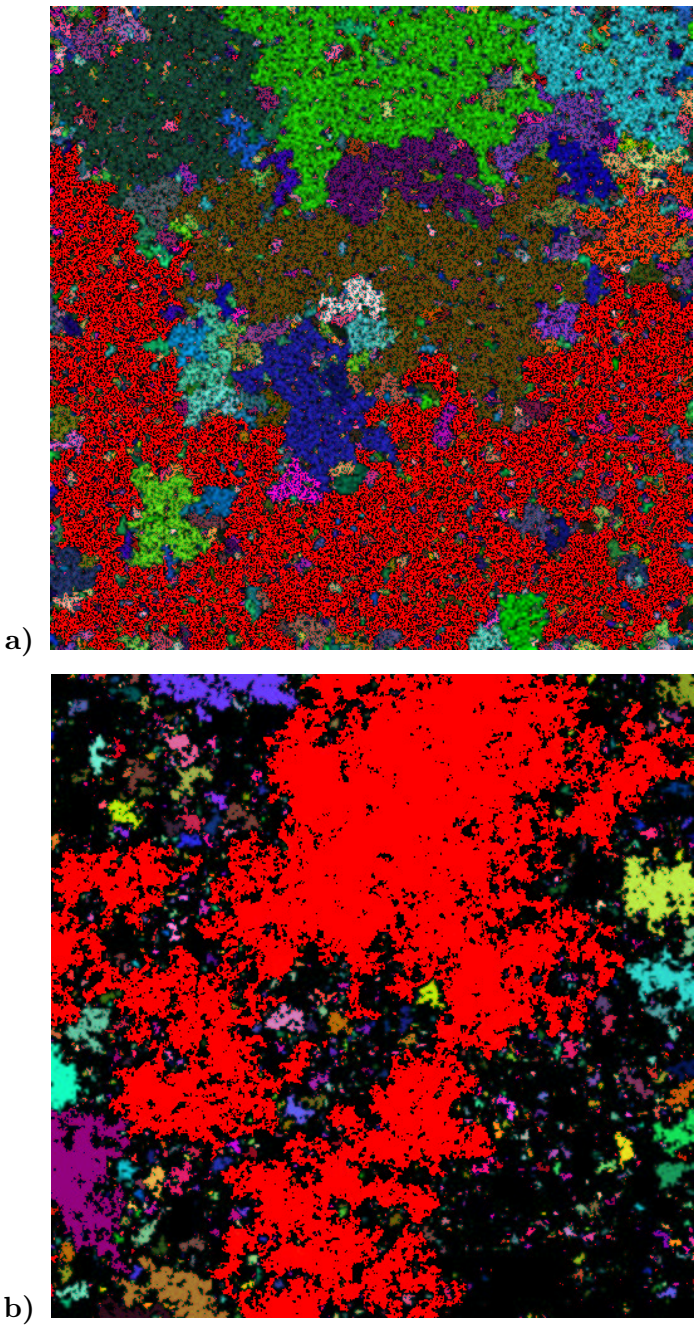

Fig. 6. Percolation at the critical concentration. a) Uncorrelated case, and b) Correlated case.

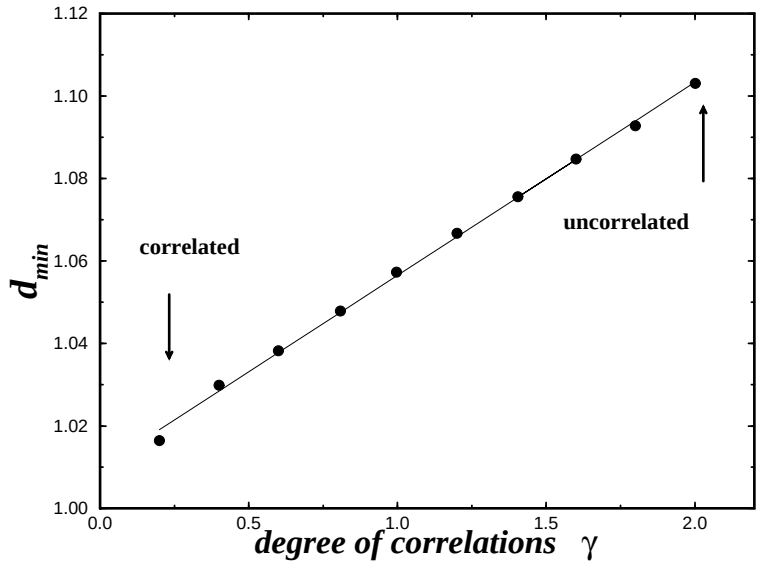

Fig. 7. Fractal dimension d_{min} as a function of the degree of correlations.

the range over which the variables are actually correlated (Prakash et al. 1992, Peng et al. 1991). Other methods present similar problems (see for instance Chapter 9 in Feder's book (Saupe 1988, Feder 1988)). As a consequence, one must generate a very large sequence of numbers, and then use only the small fraction of them that are actually correlated (this fraction can be as small as 0.1% of the initial length of the sequence (Prakash et al. 1992, Peng et al. 1991)). This limitation makes the Ffm not suitable for the study of scaling properties in the limit of large systems.

We have modified the Ffm in order to remove the cutoff in the range of correlations. We showed that in the modified method the actual correlations extend to the *whole system* (see Ref. Makse et al. 1995c).

7 Conclusions

Spatial patterns in permeable rocks exist and require quantitative methods to describe them. In the particular case of Aeolian systems (such as the Lochabriggs sample), we show that the observed periodic stratified pattern can be understood with a "table top" experiment. While these results apply only to aeolian systems, the finding of long-range correlations in sandstone appears to be true independent of the geological process involved. For the two samples studied so far it has been shown that the correlations can be well modeled using a power law.

These spatial patterns have very great consequences for prediction of, for example, hydrocarbon recovery or contaminant transport in ground water. The fact that there exist long range correlations implies that contaminant transport might be less dispersed than would be predicted from a short range correlation model.

Acknowledgements We thank P. Cizeau, G. Davies, P. Ch. Ivanov and S. Tomassone for discussions and BP for financial support.

References

Allen, J. R. L. *Journal of Geology* **78**, 326-351 (1970).
Bagnold, R. A. *The physics of blown sand and desert dunes* (Chapman and Hall, London 1941).
Bagnold, R. A. *Proc. Roy. Soc. London* **A 295**, 219-232 (1966).
Borges, J. L. *The book of sand* (Emecé, Buenos Aires 1975).
Buck, S. G., Jour. Sed. Petrology **55**, 895 (1985).
Bunde A. and Havlin, S., eds., *Fractals in Science* (Springer-Verlag, Berlin 1994).
Cheel, R. J. & Middleton, G. V. *Journal of Geology* **94**, 489-504 (1986).
Coniglio, A., Nappi C., Russo L., and Peruggi F., J. Phys. A **10**, 205-209 (1977).
Fryberger, S. G. & Schenk, C. *Sedimentology* **28**, 805-821 (1981).
Halvorsen, C. and Hurst, A., in *Advances in Core Evaluation Accuracy and Prediction*, Edited by P. F. Worthington (Gordon and Breach, 1990).
Hele-Shaw, H. S. *Nature* **58**, 34-36 (1898).
Hunter, R. E., Jour. Sed. Petrology **55**, 886 (1985).
Jaeger, H. M. & Nagel S. R. *Science* **255**, 1523-1531 (1992).
Jopling, A. V. & Walker, R. G. *Journal of Sedimentary Petrology* **38**, 971-984 (1968).
Leschhorn H. and Tang L.-H., Phys. Rev. Lett. **70**, 2973 (1993).
Makse, H. A. and Amaral, L. A. N., Europhys. Lett. **31**, 379 (1995).
Makse, H. A., Davies, G., Havlin, S. Ivanov, P. Ch., King, P. R., and Stanley H. E., Phys. Rev. E **54**, 3129 (1996a).
Makse, H. A., Havlin, S., King, P. R., and Stanley, H. E. (submitted, 1995b).
Makse H. A., Havlin, S., Stanley, H. E., and Schwartz, M. [1993 Int. Conf. Complex Systems in Computational Physics, Buenos Aires] Chaos, Solitons and Fractals **6**, 295 (1995a).
Makse, H. A., Havlin, S., Schwartz, M., and Stanley, H. E., Phys. Rev. E **53**, 5445 (1995c).
Makse H. A., Cizeau P., and Stanley, H. E. (submitted, 1996b).
McKee, E. D., Crosby, E. J. & Berryhill, H. L. JR. *Journal of Sedimentary Petrology* **37**, 829-851 (1967).
Muzy, J.F., Bacry, E., and Arneodo, A., Phys. Rev. Lett. **67**, 3515 (1991); A. Arneodo, E. Bacry, P. V. Graves, and J. F. Muzy, *ibid* **74**, 3292 (1995).
Peng, C. K., Havlin, S., Schwartz, M., and Stanley, H. E., Phys. Rev. A **44**, 2239 (1991).
Peng C. K., Buldyrev S. V., Havlin, S., Simons, M., Stanley, H. E. and Goldberger, A. L., Phys. Rev. E **49**, 1685–1689 (1994).

Prakash, S., Havlin S., Schwartz, M., Stanley, H. E., Phys. Rev E **46**, R1724 (1992).
D. Saupe in *The Science of Fractal Images*, Peitgen, H.-O. and Saupe D., eds. (Springer-Verlag, New York 1988).
Feder J., *Fractals* (Plenum Press, New York 1988).
Vicsek, T., *Fractal Growth Phenomena*, 2nd ed., Part IV (World Scientific, Singapore, 1992).
Barabasi, A.-L. and Stanley, H. E., *Fractal Concepts in Surface Growth* (Cambridge University Press, Cambridge, 1995).
Family, F. and Vicsek T., eds., *Dynamics of Fractal Surfaces* (World Scientific, Singapore 1991).
Weinrib, A., *Phys. Rev. B* **29**, 387-395 (1984).